

Recent Photonics Activities Under the NASA Electronic Parts and Packaging (NEPP) Program

Charles Barnes*, Melanie Ott**, Allan Johnston*, Ken LaBel**, Robert Reed**, Cheryl Marshall** and Tets Miyahira*

*Jet Propulsion Laboratory, California Institute of Technology

**NASA Goddard Space Flight Center

ABSTRACT

With the rapidly increasing insertion of photonic devices, circuits and subsystems into NASA spacecraft, a variety of issues associated with reliability and radiation tolerance have arisen. In this paper, we discuss these issues from the perspective of the work currently ongoing in the NASA Electronic Parts and Packaging (NEPP) Program. This Program is focused on evaluating the reliability and radiation response of advanced and emerging microelectronics and photonics technologies of interest to NASA spacecraft system designers. Examples to be discussed include radiation studies of various optoelectronic devices and reliability of photonic components. These studies have been motivated in part by problems observed in space that include the failure of optocouplers on TOPEX/Poseidon, and the observation of single event-induced transients in the Hubble Space Telescope.

1. INTRODUCTION

The qualification of microelectronic and photonic devices for space applications is challenging and difficult because the space environment presents a variety of stressing factors that these devices must survive so that mission success is not jeopardized. As shown in Figure 1 for the various phases of a typical Mars mission, these environmental factors include a wide variety of effects that can cause photonic devices and circuits to degrade and possibly fail completely. Several of these environmental effects are always present in a NASA mission, such as vibration effects during launch, but the dominant, most severe effect can vary dramatically depending on the mission scenario. Unlike missions to the Jovian system where radiation is usually the dominant factor, total ionizing dose (TID) is relatively low for Mars missions such as that in Figure 1, and low temperature effects and contamination, especially for Marian surface assets, can be very important. In contrast, for low Earth orbit (LEO) missions, such as the International Space Station (ISS) and the Shuttle, solar flare-induced radiation effects, both TID and single event effects (SEE), and aging effects for long missions are often significant. The important point to be made, however, is that space qualification of photonics for all NASA missions is difficult and challenging, especially for commercial off-the-shelf (COTS) photonic components which are not intended for use in the space environment.

The NASA Parts and Packaging (NEPP) Program is a NASA multi-Center Program whose objective is to assess the reliability and radiation tolerance of newly available COTS and emerging electronic and photonic parts and packaging technologies in order to facilitate the low-risk insertion of microelectronics and photonics technologies in NASA systems. In meeting this objective, the NEPP Program evaluates a wide variety of photonics components including optocouplers, LEDs, laser diodes, optical fibers, modulators, detectors, fiber optic links and accompanying conditioning and amplification electronics. These evaluations take into account those environmental parameters that can adversely affect the performance of these photonic components. As indicated in Figure 1, these include operation at very low temperatures, exposure to different types of radiation, damage and misalignment due to mechanical shock and vibration, aging effects and thermal cycling. In this paper, we provide a few recent examples of this work.

*charles.e.barnes@jpl.nasa.gov; phone (818) 354-4467; FAX (818) 393-4419; Jet Propulsion Laboratory, 4800 Oak Grove Drive, M.S. 303-202, Pasadena, CA 91109

**melanie.n.ott.1@gsfc.nasa.gov; (301) 286-0127; FAX (301) 286-1695; NASA, Goddard Space Flight Center, M.S. 562.0, Greenbelt, MD 20771

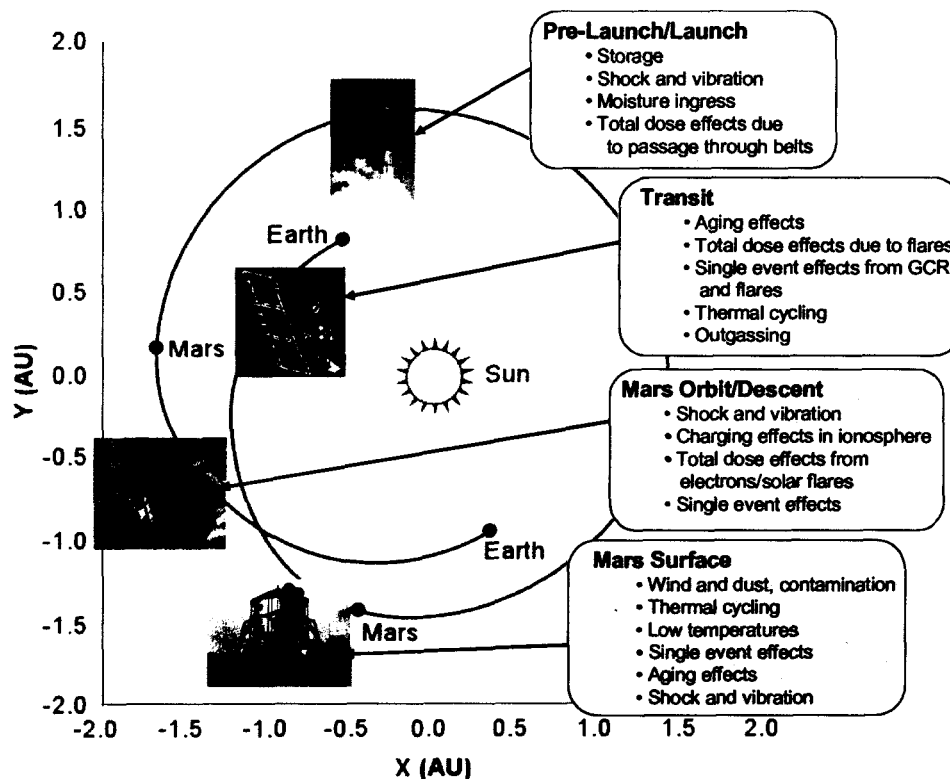


Figure 1. Impact of various space environmental factors on photonic devices for a typical Mars mission scenario.

2. RADIATION EVALUATIONS

Photonic components are susceptible to a variety of radiation effects which can degrade their performance during a space mission, leading to reduced performance of spacecraft engineering systems or loss of science data from science instruments. In addition, combinations of radiation with other environmental factors can lead to strong, negative synergistic effects. For example, radiation tolerance is often much less at low temperature, and aging effects late in a mission can reduce the margin available to accommodate radiation-induced reductions in performance. In spite of a long history¹ of investigation of radiation effects in photonics, there are still many issues and problems to be solved prior to using photonics in mission scenarios that have significant radiation exposure. This is true primarily because of the continual evolution of photonic technologies and the introduction of entirely new technologies. In subsequent Sections we provide examples of some recent work in this area under the NEPP Program.

2.1 Proton-Induced Displacement Damage in Optocouplers

Early investigations² of optocoupler radiation sensitivity under the NEPP Program were prompted by optocoupler failures observed on the TOPEX/Poseidon satellite, as shown in Figure 2. These failures occurred in thruster status electronic circuits, beginning at a little more than two years after launch. Fortunately, the status circuit failures did not impact actual thruster operation.

The TOPEX/Poseidon optocoupler failures brought to light an important radiation hardness assurance (RHA) issue. Typical radiation testing of optocouplers had been done using Co-60 gamma ray sources to establish total ionizing dose (TID) susceptibility limits of these devices. Because optocouplers and their components are primarily susceptible to displacement damage, their Co-60-determined TID resistance levels are quite high since gamma rays cause negligible displacement damage. The TOPEX/Poseidon failure levels, observed at much lower dose levels, suggested that protons in the space environment caused the primary effect, and this was verified by comparing 4N49 optocoupler Co-60 response with that to protons². These results are shown in Figure 3; which shows the greater sensitivity to protons.

Thruster	Days after Launch										
	23	35	63	133	231	360	538	647	786	1014	1252
A2-A	ok	ok	-	-	-	-	-	-	-	-	F
A2-B	ok	ok	-	-	-	-	-	-	-	-	F
C3-A	ok	ok	-	-	-	-	-	-	-	-	F
C3-B	ok	ok	-	-	-	-	-	-	-	-	F
A4-A	-	ok	ok	ok	ok	ok	ok	ok	F	F	F
A4-B	-	ok	ok	ok	ok	ok	ok	ok	F	F	F
C4-A	-	ok	ok	ok	ok	ok	ok	ok	ok	ok	F
C4-B	-	ok	ok	ok	ok	ok	ok	ok	F	F	F

First failures occur at
 $1.4 \times 10^{10} \text{ p/cm}^2$

Figure 2. Thruster status circuit optocoupler failures on the TOPEX/Poseidon satellite.

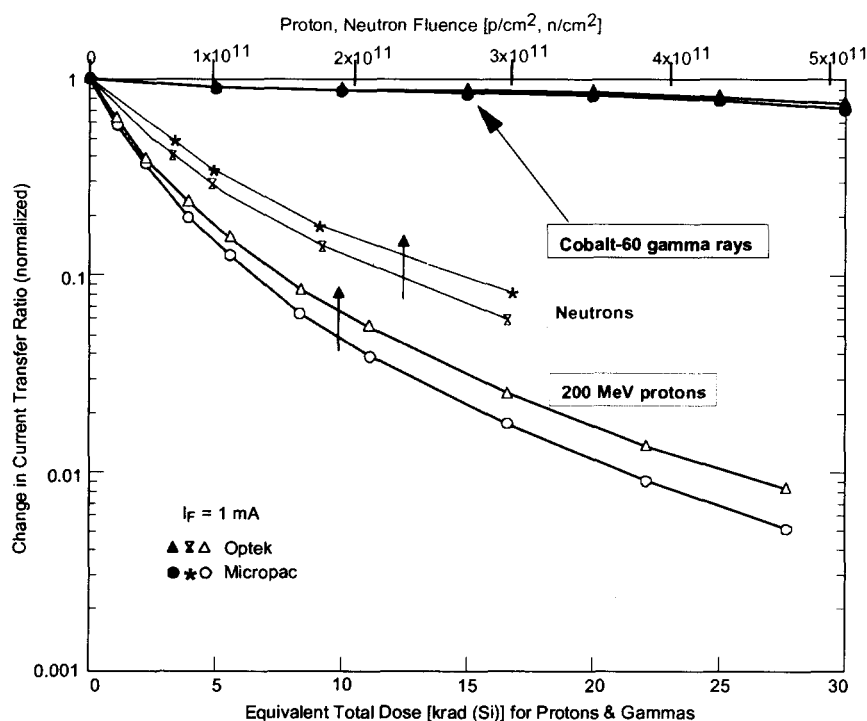


Figure 3. Radiation sensitivity of 4N49 optocouplers to neutrons, protons and Co-60 gamma rays. Note the much greater sensitivity to protons and neutrons, which is attributed to the dominance of displacement damage in the optocoupler degradation, as opposed to ionization effects caused by gamma rays. Current transfer ratio (CTR) is the ratio of optocoupler output current to input current.

In addition to the necessity for using the proper type of radiation (protons for displacement damage effects) to establish RHA, the determination of the overall radiation susceptibility of optocouplers is complicated by the fact that optocouplers contain components, LEDs and detectors, that exhibit different and varying radiation sensitivities. In the case of proton-induced displacement damage, typical results for the varying sensitivity of optocoupler components is shown in Figure 4 for 4N49 optocouplers. The total degradation is made up of that due to both the LED and the detector. Note that for this particular case, the LED is significantly more sensitive to damage than the detector. In the next Section we will present additional discussion of LED effects.

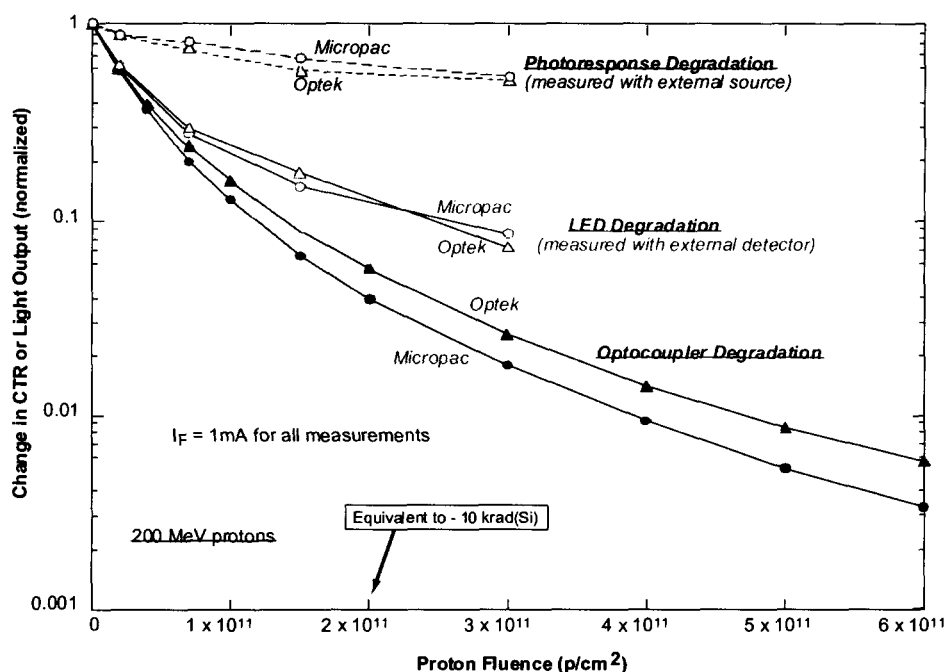


Figure 4. Proton-induced displacement damage degradation of 4N49 optocoupler components.

More recent NEPP Program investigations³⁻⁶ of displacement damage effects in optocouplers have shown that the 4N49 is one of the most sensitive devices, and that more advanced, high speed couplers are more resistant to displacement damage. For example, in Figure 5 data are shown for the current-dependent proton-induced degradation in CTR for an advanced optocoupler from Agilent. Note that, in comparison with the 4N49 in Figures 3 and 4, the radiation hardness is much greater for the Agilent device. In addition the CTRs for the Agilent devices are significantly larger than for the 4N49s. The recent summary of results by O'Bryan, et al⁵ indicates that there is considerable variation in the displacement damage hardness levels for available optocouplers. Not only is optocoupler selection for space missions complicated by these variations and the complexity of the radiation response, but for COTS optocouplers, as is often true for COTS digital and analog Si microcircuits, the radiation response of a given device type from a given manufacturer can vary with date of purchase as shown in Figure 6 for 4N49s from Micropac. The implication of these data is that one must radiation test each flight lot when using COTS optocouplers.

2.2 Light Emitting Diodes (LEDs)

Very often, a major fraction of the displacement damage sensitivity exhibited by optocouplers, such as those in Figures 3 and 4, is due to degradation of the LED portion of the optocoupler. For this reason, extensive studies have been undertaken within the NEPP Program of displacement damage effects in a variety of LEDs. The recent proton irradiation data shown in Figure 7 illustrates this variation in radiation sensitivity⁷. Note that the longer wavelength amphotERICALLY doped (N and P-type dopants are both Si) GaAs LEDs are significantly more sensitive to proton-induced displacement damage than the shorter wavelength Optodiode and Hamamatsu LEDs. The greater radiation sensitivity of the amphotERICALLY doped LEDs has been attributed to differing current flow mechanisms and also basic differences in radiative recombination mechanisms⁷. Basic physics aside, the primary concern for the space application user is the type of LED used in COTS optocouplers selected for these applications. In NASA applications, there have been instances when COTS optocoupler manufacturers switched LED types within their optocouplers without informing users, leading to increases in radiation sensitivity of the optocouplers. Thus, it is important to determine the type of LED used in the optocoupler flight lot and if at all possible, avoid the use of optocouplers with amphotERICALLY doped LEDs. An alternative solution to the problem of optocoupler LED radiation susceptibility, is to work with the optocoupler manufacturer to develop requirements and specifications for a radiation tolerant LED as an optocoupler component. This has been accomplished recently by specifying a double heterojunction hardened LED that lead to an order of magnitude improvement in optocoupler radiation resistance⁴.

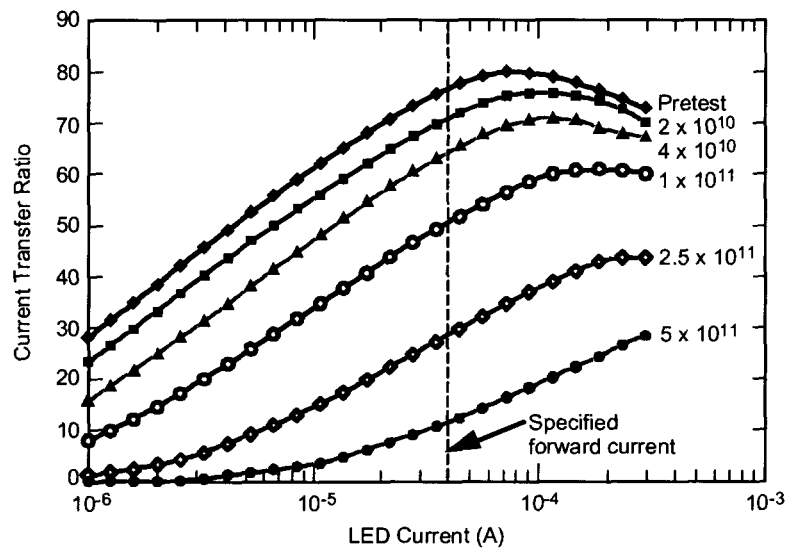


Figure 5. Proton-induced degradation in CTR for Agilent HCPL-4701 optocouplers as a function of input LED current. Proton fluences in p/cm^2 are shown at the right of each curve.

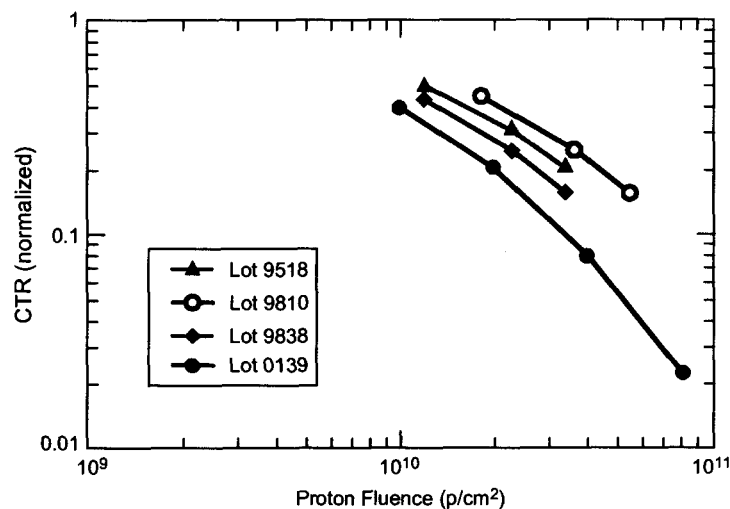


Figure 6. Variation of radiation response for different lots of Micropac 4N49 optocouplers over a seven year period.

Selection of LEDs and optocouplers for use in space applications is further complicated by the complexities involved in extrapolating ground radiation test results to the actual space environment. As indicated in Figure 7, proton testing for displacement damage effects is usually done at only one proton energy to establish RHA for LEDs and optocouplers. However, protons in the space environment are characterized by a wide energy spectrum, and the efficiency by which displacement damage is created in semiconductor devices is dependent on proton energy. Reed, et al⁸ have measured the energy dependence of proton-induced LED degradation, and analyzed the results within the framework of expected non-ionizing energy loss (NIEL) in GaAs/AlGaAs in order to develop a method of extrapolating test results to the space environment. Representative results are shown in Figure 8 for single heterojunction LEDs irradiated at different proton energies and accelerator facilities. The solid line represents a theoretical NIEL calculation for GaAs. Note that when the data is normalized to the NIEL calculation at 10 MeV proton energy, it agrees with the calculation at low and mid-energies but deviates significantly at high energies. However, as shown in Figure 8, the experimental NIEL data of Barry, et al⁹ agrees well with the single heterojunction data and also that for double heterojunction LEDs (not shown). As demonstrated by Reed, et al⁸, this agreement can form the basis for more accurate prediction of expected damage in space.

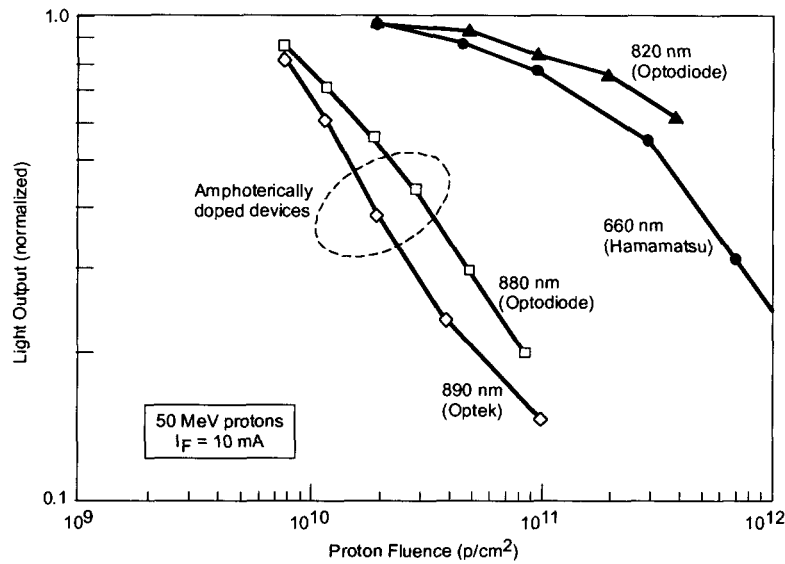


Figure 7. Proton-induced displacement damage degradation of four types of LEDs at moderate current levels.

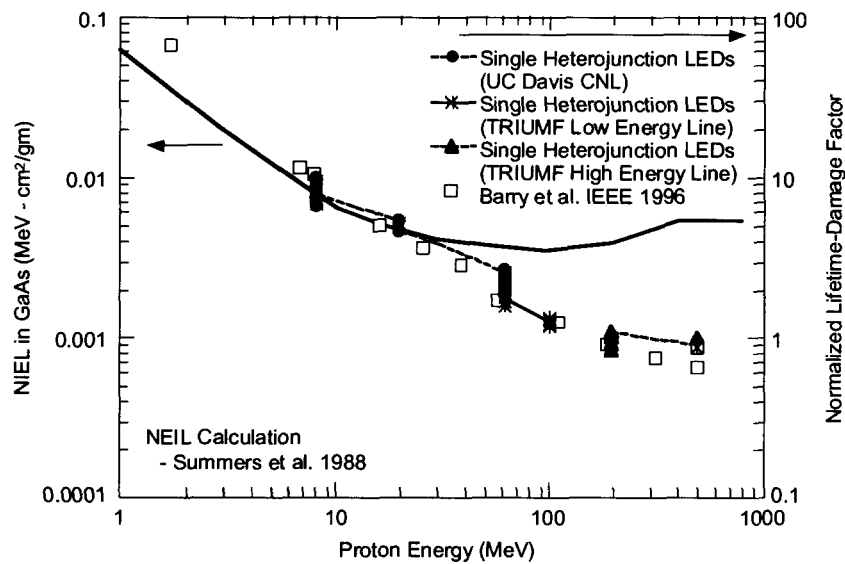


Figure 8. LED degradation, expressed as lifetime-damage factor, normalized to agree with calculated NIEL values for 10 MeV protons.

2.3 Single Event Effects in Optocouplers

In addition to proton-induced optocoupler displacement damage effects, in themselves relatively complex, single event effects (SEE) also affect the performance of optocouplers, and can compound the RHA issues for these devices. While LEDs usually dominate the response to displacement damage effects in optocouplers, SEE occur in the detector portion of optocouplers, and also in fiber optic link (FOL) receivers. The SEE of concern are single event transients (SETs) that can produce large pulses of photocurrent that will disrupt optocoupler and FOL functionality. The occurrence of SETs is not surprising since detectors are intended to transform electromagnetic radiation in the form of light emitted by the LED into photocurrent. Thus, protons, electrons and the heavy ions making up galactic cosmic rays (GCRs), all of which produce more intense ionization tracks than light, can be expected to cause large photocurrent pulses in detectors. Of particular interest are protons because they are more plentiful than GCRs and they cause significantly greater ionization than electrons.

A simple depiction of the mechanisms for proton-induced SETs is shown in Figure 9, along with a typical proton-induced photocurrent pulse. The flat disks schematically represent the active regions in the detector structures, which for detectors appropriately designed for radiation environments are quite thin, often less than a few microns. In the case of Si detectors, it is important to avoid diffusion limited carrier collection and confine photocurrent generation to the depletion region. For a thin collection region, characteristic of the depletion layer in a relatively heavily doped junction, protons do not deposit enough energy to generate a significant pulse when traversing the collection region, that is the thin disk in Figure 9, at an angle to the large flat surface of greater than about 10° to 15° . Thus, there are two effective mechanisms for creating large photocurrent pulses that can disrupt circuit function: 1) as shown at the top, when the proton traverses the active region along a path close to parallel to the surface (direct interaction), and 2) when there is a nuclear reaction resulting in recoils that create heavy charge, as in the bottom illustration. Consequently, for direct interaction one expects a strong angular dependence. As shown in Figure 10, this direct interaction model has been borne out by observations of strong angular dependence of SETs^{3,5,10}.

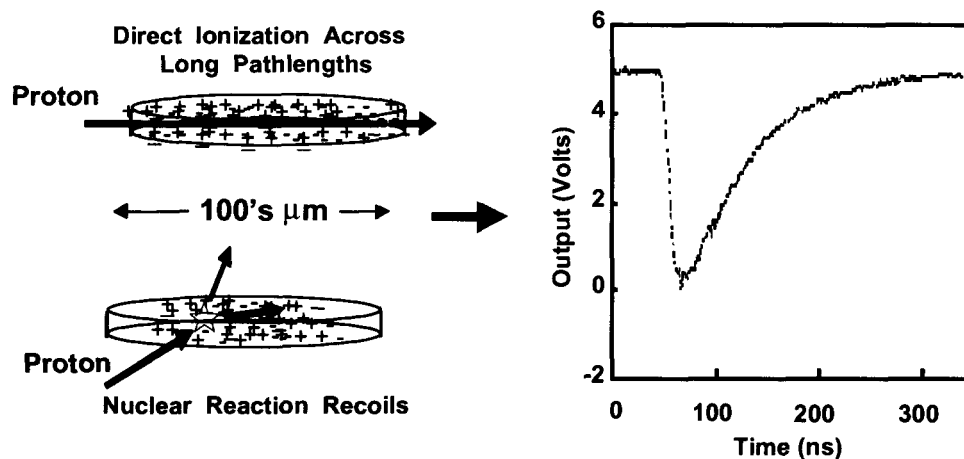


Figure 9. Model for two mechanisms for proton-induced single event transient photocurrent pulses as shown at the right.

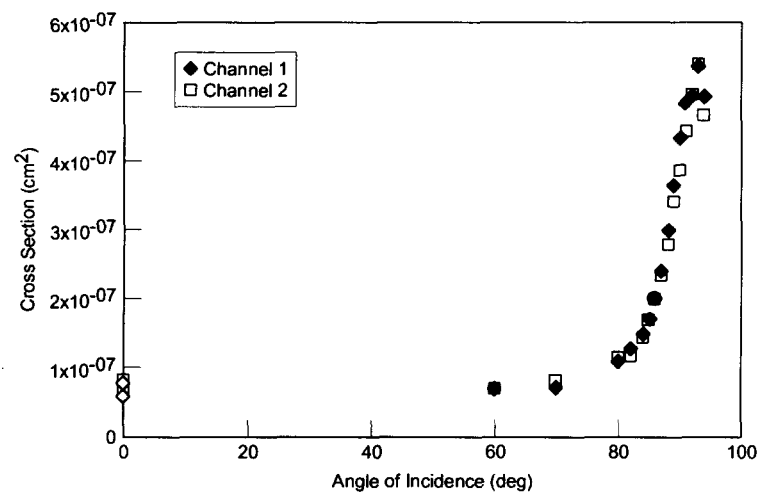


Figure 10. Angular dependence of proton-induced SETs.

It has also been shown^{3,10,11} that the cross section for SET production decreases strongly with increasing optical power impinging on the detector in an optocoupler or on the FOL receiver. The SET cross section also depends on data rate, and is greater in faster, high speed optocouplers and FOLs. These dependencies and various filtering techniques can be used to mitigate SETs and prevent them from producing false output signals in optocouplers and high speed FOLs.

2.4 Radiation Effects in Injection Laser Diodes (ILDs)

Proton-induced displacement damage also degrades the behavior of injection laser diodes (ILDs). Recent data¹² illustrating this effect is shown in Figure 11 for Mitsubishi ILDs operating at a wavelength of 1550 nm. Note there are three regions of interest: 1) below the laser threshold current, the ILD behaves essentially like an LED and the output degrades similar to other LEDs, as in Figure 7, 2) near threshold the light output increases very rapidly with the transition into lasing, and the threshold current increases with increasing proton fluence, and 3) well into laser saturation the devices are insensitive to proton irradiation because the radiative lifetime is extremely short so that displacement damage-induced non-radiative recombination cannot compete effectively with laser output. With regard to radiation sensitivity, the most critical ILD parameter is the laser threshold current. If the proton damage causes a large increase in threshold current to a level above the maximum permissible device current then the ILD cannot be "turned on". Thus, for space applications with large expected proton fluences it is important to select ILDs with a wide current range between threshold and maximum operating current. The variation of threshold current with proton fluence for four different ILDs is shown in Figure 12.

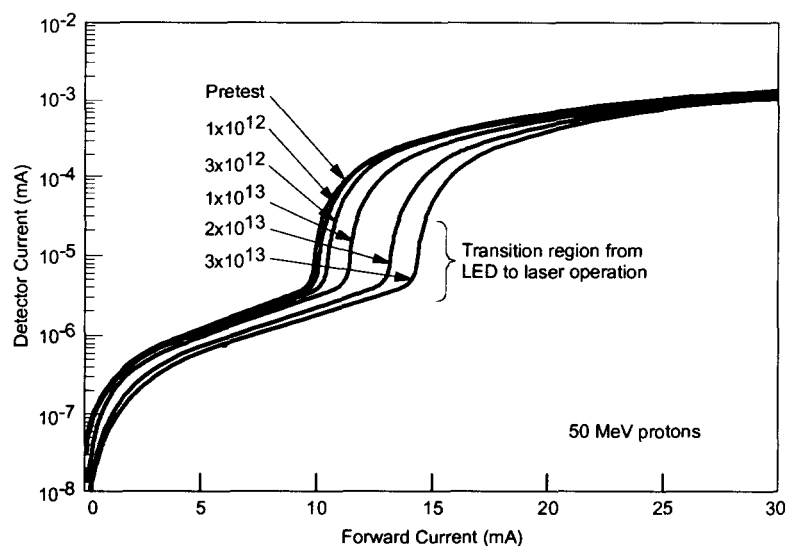


Figure 11. Proton-induced displacement damage degradation of Mitsubishi 1550-nm ILD.

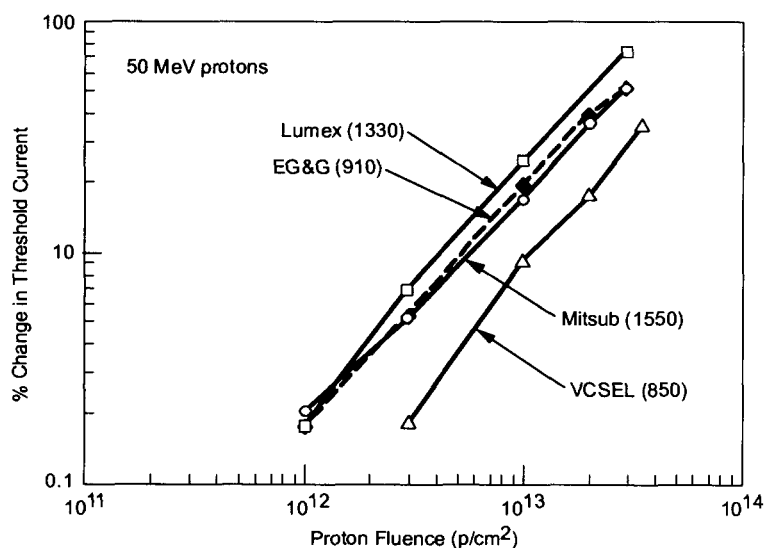


Figure 12. Proton-induced increase in ILD threshold current for four types of lasers.

As a possible method of damage mitigation in ILDs, one may be able to take advantage of a relatively unique annealing phenomenon. Degraded ILDs are often observed to recover during forward current bias without any need for heating to induce thermally stimulated annealing. Examples¹² of this non-thermal annealing effect are shown in Figure 13 for a 1300-nm ILD. Note that if the ILD is unbiased at room temperature, there is no recovery of threshold current, but when the device is placed under forward bias the recovery is substantial. This non-thermal annealing effect, termed recombination enhanced annealing, is due to the transfer of energy from a non-radiative recombination event at a displacement damage-induced non-radiative recombination defect center to lattice phonon energy. In GaAs and AlGaAs, the energy band gap is wide enough so that this lattice photon energy is sufficient to cause the defect to jump from one lattice site to another thus resulting in an annealing effect. One can envision exploiting this annealing effect by merely turning on the laser during the mission after exposure to significant proton fluences.

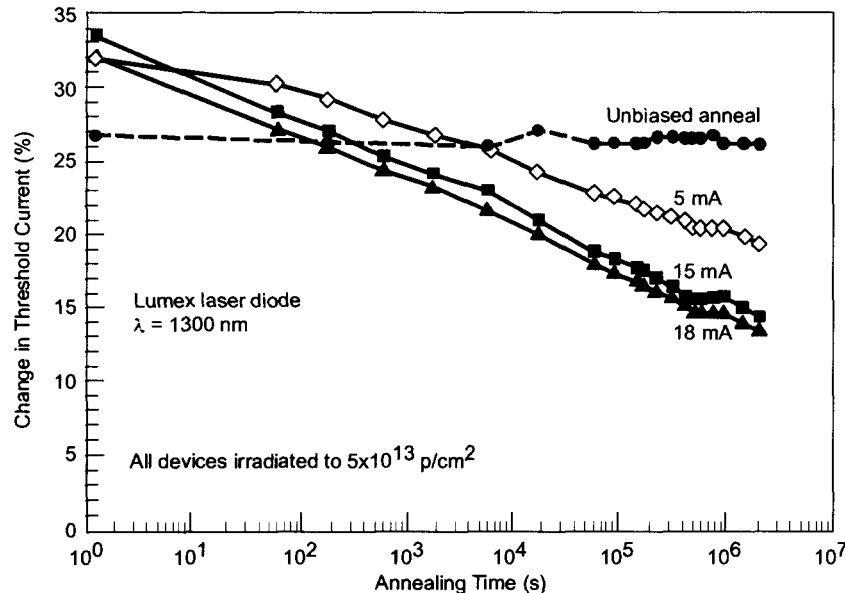


Figure 13. Forward current-induced annealing of displacement damage in 1300-nm emitting ILDs.

2.5 Fiber Optic Cables

The effects of radiation on optical fibers and cables have been investigated over many years¹³, but RHA issues still remain for application of fiber cables in NASA missions. The focus of work in the NEPP Program has been on fiber cables for use in the International Space Station (ISS) and the behavior of high speed FOLs for future use in NASA systems^{14,15}. There is a parallel between Si microcircuits and optical fibers in the sense that radiation hardened microcircuits have become difficult to obtain so that space system designers have had to resort to COTS Si digital and analog microcircuits. Similarly, optical fibers hardened for the space environment have become very difficult to find, and this has required additional radiation testing of COTS fiber cables to determine their radiation tolerance. A recent example of this work is shown in Figure 14 for total dose testing of a COTS graded index, germanium doped fiber cable manufactured by Lucent. As shown in Figure 14, 100 m lengths of fiber were irradiated at different relatively low dose rates and at two temperatures, +25°C and -25°C, with fiber attenuation measurements at a wavelength of 1300 nm. The total dose-induced attenuation in these fibers is due to the introduction of germanium-related color centers which is offset during irradiation by the annealing of these centers. The balance between the radiation-induced color center production rate and the color center disappearance due to annealing is influenced by several factors including fiber core doping level, fiber drawing characteristics, dose rate and temperature. Generally, the balance is shifted toward greater attenuation for higher dose rates and lower temperatures, in agreement with the data in Figure 14. As is often the case with doped fibers, the attenuation growth is essentially linear with irradiation time and does not exhibit saturation. It is interesting to note that the dose rate has relatively greater influence on the attenuation than does temperature suggesting that the annealing rate is significant and not particularly dependent on temperature. We also note that the induced attenuation is quite high in these fibers; of the order of 0.4 dB/m at 30 krad/s at a dose rate of approximately 0.5 rad/s.

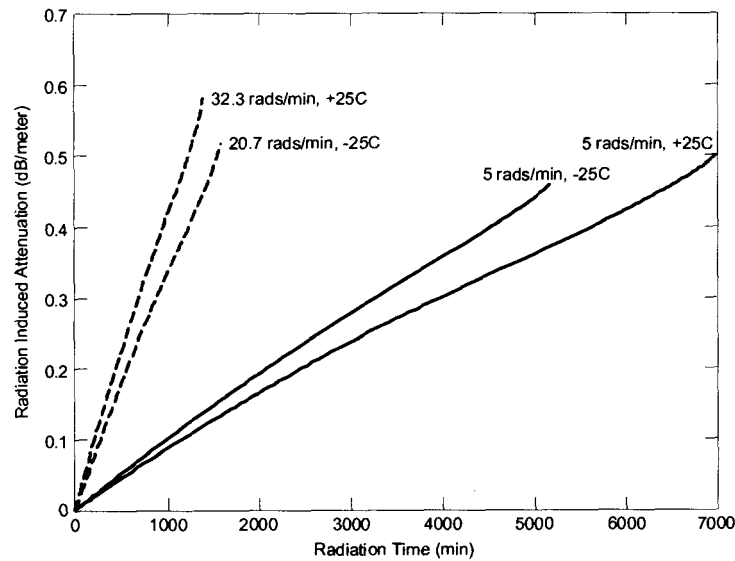


Figure 14. Total dose-induced attenuation at 1300 nm in COTS graded index, germanium doped fiber cable manufactured by Lucent.

The results shown in Figure 14 indicate that the Lucent fiber is relatively sensitive to radiation so that for lengths greater than 10 m this fiber is not the best choice for applications that require high performance. However, at low dose rates, low total doses and short lengths, this fiber can perform with less than 1 dB of loss. For 1 rad/min at 10 Krads the losses at -25°C for 3 meters of fiber (typical length used) are less than 0.5 dB and at $+25^{\circ}\text{C}$ the losses with these same conditions are less than 0.3 dB. Thus, in relatively benign radiation environments that do not require very low temperature operation the Lucent commercial 62.5/125 micron fiber can provide a suitable solution in lengths less than 10 m. For those applications with more stringent radiation and temperature requirements and relatively long fiber lengths, a step index fiber with undoped core would be more appropriate if the data rate is not too high. In any case, the use of COTS fiber cables in the space environment requires thorough testing in order to insure sufficient RHA, similar to the case for use of COTS Si microcircuits in the space environment.

2.6 Fiber Optic Links (FOLs) in Space

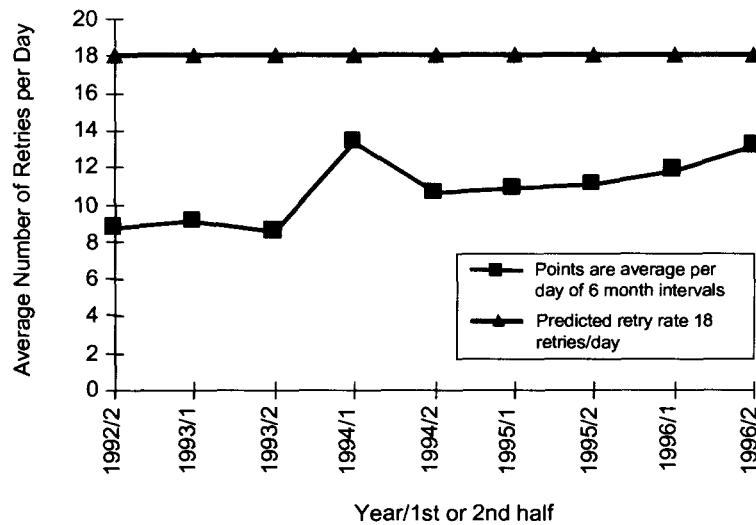
Under the NEPP Program, evaluations have been performed on a wide variety of FOLs with speed performance from the 1 MHz to multi-GHz regimes, and have included investigations of different optical receiver technologies, wavelengths, and designs, and various system parameters such as data rate and optical power budget. All of these factors and more play a significant role in predicting an FOL's bit error rate (BER) performance in space. These evaluations have been done in support of present and future insertion of FOLs in NASA flight systems. FOLs currently in flight are shown in Table 1.

Table 1. Current fiber optic links in space.

PROJECT	LAUNCH	TECHNOLOGY	SYSTEM WAVE LENGTH
SAMPEX	7/92	MIL-STD-1773 1Mbps	850nm
MPTB	12/97	AS1773 20Mbps	1300nm
MAP	2000	AS1773 20Mbps	1300nm
XTE	12/96	MIL-STD-1773 1Mbps	850nm
HST	02/97	MIL-STD-1773 1Mbps	850nm

The SAMPEX 1773 data link has been in operation for 10 years and has been supported by extensive ground testing and analysis of the link and its response to SETs in the link receiver. As indicated in a previous Section, detectors and receivers are particularly sensitive to SETs, and as shown in Figure 15, the SAMPEX 1773 link has been experiencing about 10 to 15 bus retries/day over the 10 year period due to SETs in the receiver. The analysis and modeling of link behavior led to the prediction of 18 retries/day, shown in Figure 15, that is close to the actual observed retry rate. In addition, these efforts led to the development of a robust system-level mitigation that involves detection of a corrupted data transfer followed by the option of attempting a retry of the message. During a seven year flight period this retry protocol failed only once. This extensive body of work has also produced FOL assessment tools and guidelines for mitigating radiation effects in FOLs.

As noted in an earlier Section, Si detectors are susceptible to SETs because their active regions are relatively thick. Thus, in the case of a "first window" (800 nm to 850 nm) system, as for SAMPEX, one expects a relatively high SET rate in the receiver. This has led to the use of links at longer wavelengths, such as those for MPTB and MAP (Table 1), that employ III-V-based detectors such as InGaAs, which have much thinner active regions and are not as prone to SET-induced false signal pulses.



Retry = SEU in 1773 photodetector

Figure 15. SAMPEX fiber optic 1773 bus retry rates between 1992 and 1996 due to SETs in the link receiver. The gradual increase in actual retry rates is attributed to the transition from solar max to solar min during this period.

3. RELIABILITY EVALUATIONS

Under the NEPP Program, a significant amount of work has been done in the general area of the reliability, characterization and qualification of photonics components, such as optocouplers, LEDs, ILDs, large laser arrays, connectors, fiber cables and detectors, for the space environment. These investigations have led to the publication of several papers and guidelines which are helpful to the space application user¹⁶⁻²⁵. In this Section we briefly present a few examples of this work.

In support of ISS, problems associated with optical fiber jacketing and fiber cable configurations have been investigated. During the development of the ISS fiber cable harnessing, it was discovered that thermally induced cable component shrinkage was a serious issue for cables that would be used in changing thermal environments. As shown in Figure 16, several cable types were subjected to thermal cycling to investigate cable shrinkage resulting from the cycling tests. Cables were tested up to 60 thermal cycles from -30°C to 140°C at 1°C/min with a 5 min dwell at both temperature extremes. Note that all cables exhibit some shrinkage after a few 10s of cycles. Fiber cables from two manufacturers were also optically monitored to detect the effect of shrinkage on attenuation of the fiber cables, and as shown in Figure 17, the Northern Lights cable showed a definite reduction in output power with increasing number of thermal cycles.

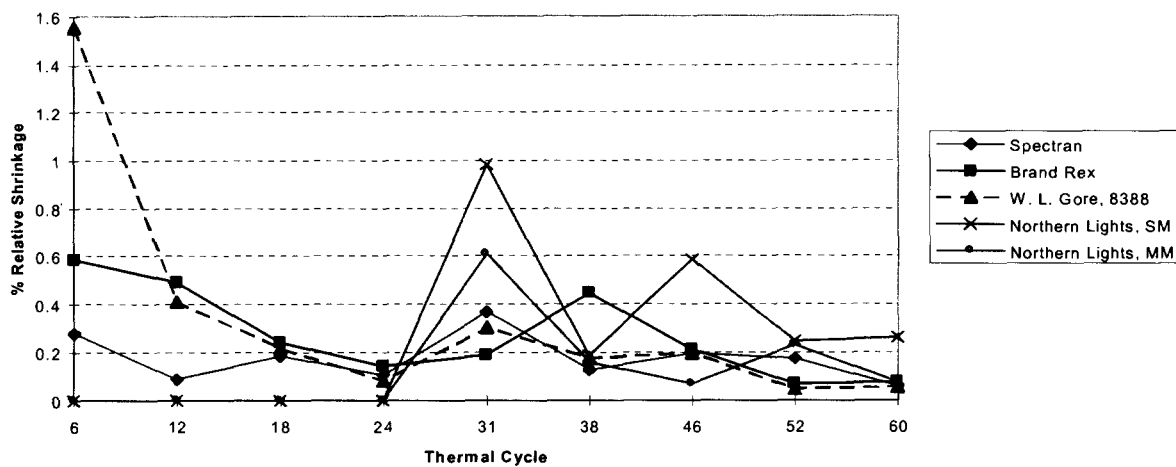


Figure 16. Thermal cycling-induced relative shrinkage in various fiber optic cables.

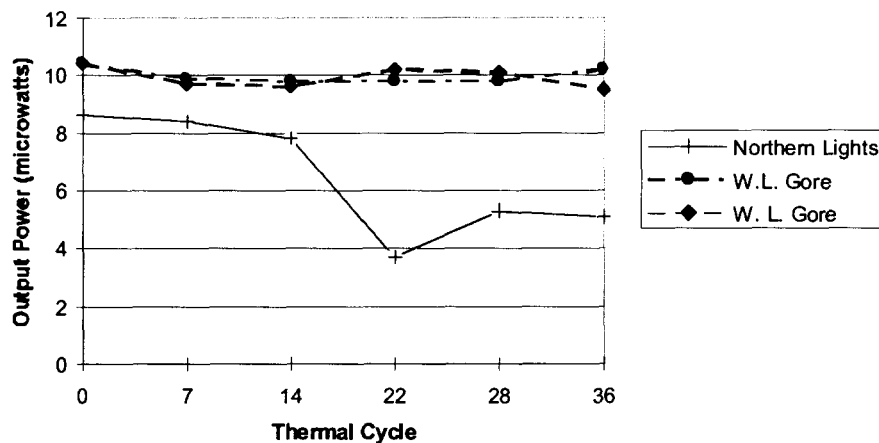


Figure 17. Optical power variation in two fiber cable types due to thermal cycling-induced cable shrinkage.

In a later study, several additional commercially available cable configurations were tested for shrinkage due to thermal cycling and compared to NASA heritage space flight cables. The thermal cycling protocol for these tests was more stringent with a temperature range from -55°C to $+125^{\circ}\text{C}$ and ramp rates of $2^{\circ}\text{C}/\text{min}$ with dwells of 28 minutes per temperature extreme. Results from these studies for five different fiber cables are shown in Figure 18. The insight gathered from this experiment proved that 20 cycles of “preconditioning”, a technique for avoiding the very high shrinkage observed early in the thermal cycling test, may not be adequate for averting this thermally induced failure mode. It was also important to note that the NASA heritage OC1008 cable was outperformed by other cables in terms of stability and thermal range. This proved of great interest to the Geoscience Laser Altimeter System (GLAS) Project since it was during this time that part selection was necessary for this mission.

In other investigations, extensive reliability studies^{16,26} have been made of a 12 channel optical fiber connector assembly in support of the development of the Spaceborne Fiber Optic Data Bus (SFODB) for future NASA flight missions with intensive communications and data transfer requirements. Initial studies were performed on a commercial version of the 12 channel optical fiber ribbon cable assembly with MTP array connector. The results of this effort led to suggestions for modifying the assembly to make it more reliable, and the modified assembly was the object of follow-on reliability tests. The modifications involved two enhancements applied to the earlier technology to better suit the vacuum environment and increase the reliability of the assembly during vibration. The MTP assembly characterized here has a 100/140 optical commercial fiber and non-outgassing connector and cable components.

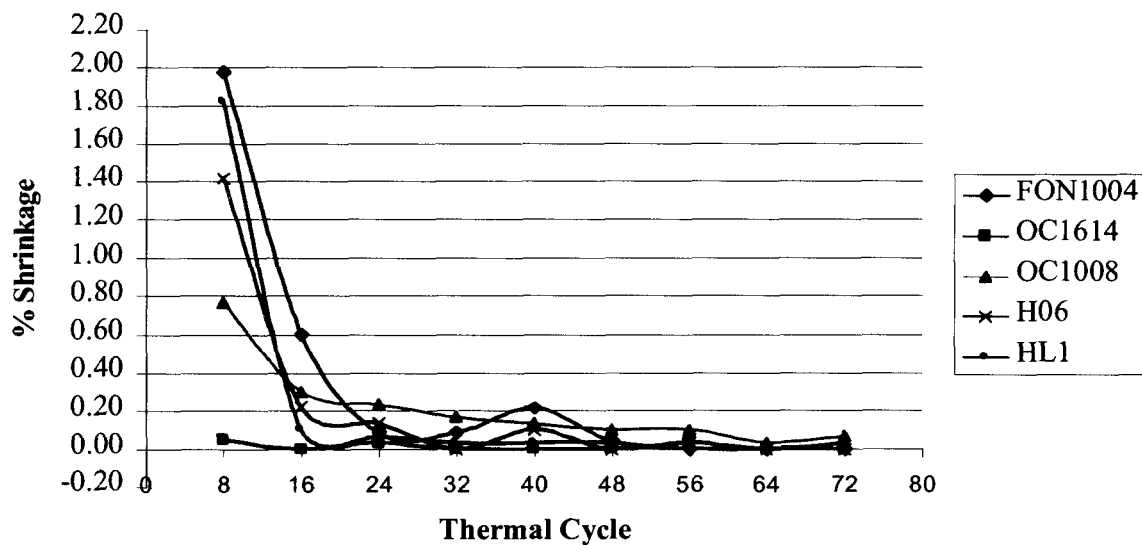


Figure 18. Thermal cycling-induced shrinkage in five different COTS fiber cables.

The modified assemblies were subjected to vibration and thermal cycling tests. During these tests, a 1310 nm laser source was used to monitor optical power throughput for selected channels of the 12 channel array in order to determine the effects of these environments on the optical power transmission. The parameters of the vibration tests were based on typical launch conditions for components under prototype testing. Three assemblies were subjected to vibration tests in x, y and z directions, each for a duration of 3 minutes, as defined in Figure 19. The results of these tests for vibration in the three directions are shown for one assembly in Figures 20, 21 and 22. Because an optical power meter was used to monitor most of the channels, the results shown in these three Figures are “quasi-static” because the meter did not follow the vibrations in real time. Note that the optical power variation is both positive and negative relative to the pretest power level. For all three tested assemblies and all three vibration axes, the quasi-static losses never exceeded 0.5 dB for any of the channels tested, and as verified through visual inspection, none of the optical fiber interfaces were damaged as a result of the vibration launch conditions used in these tests.

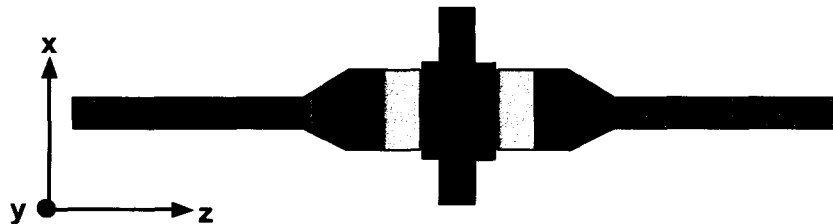


Figure 19. Orientation of MTP twelve channel ribbon connector assembly for vibration testing.

The modified assemblies were also subjected to thermal cycling tests with active optical power monitoring as in the vibration tests. The thermal cycling parameters were 38 cycles maximum, from -20°C to $+85^{\circ}\text{C}$, with a ramp rate of $1^{\circ}\text{C}/\text{min}$ and dwell times at the extremes of 25 minutes. For all three assemblies and all monitored channels, the maximum optical transmission change observed during a single cycle was 1.6 dB, and the maximum change observed during an entire thermal cycling test was 1.8 dB. Typical results for one of the assemblies are shown in Figure 23. Note that initially there is a drop in optical transmission followed by a recovery during thermal cycling to an average optical transmission near that for pretest conditions. It is interesting to note that the general shape of these results is similar to the thermal cycling-induced shrinkage data shown in Figures 16 and 18 in that there is a large initial change followed by a damping out of this change. Following the vibration and thermal cycling tests, all end faces in all the assemblies were inspected and no damage was found. These results indicate that these assemblies are appropriate for space applications as part of the SFODB.

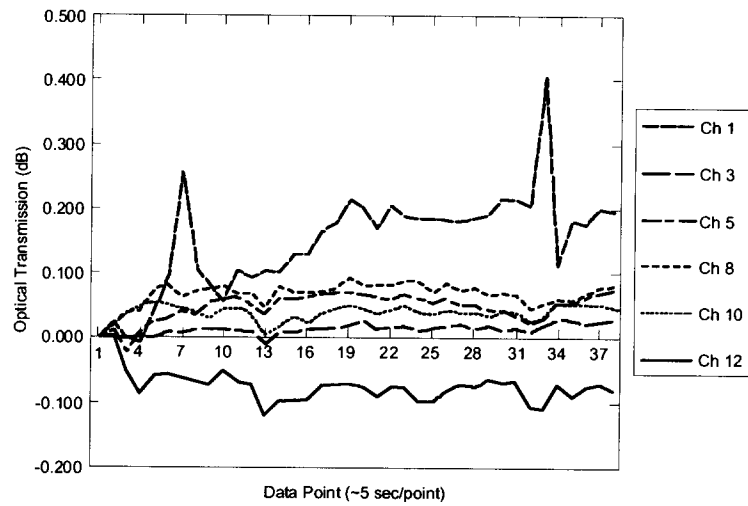


Figure 20. *In situ* optical power transmission during X-axis vibration of MTP connector assembly.

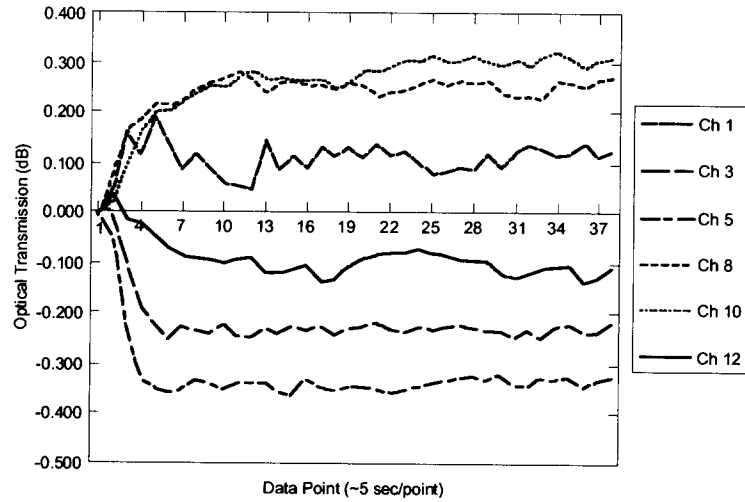


Figure 21. *In situ* optical power transmission during Y-axis vibration of MTP connector assembly.

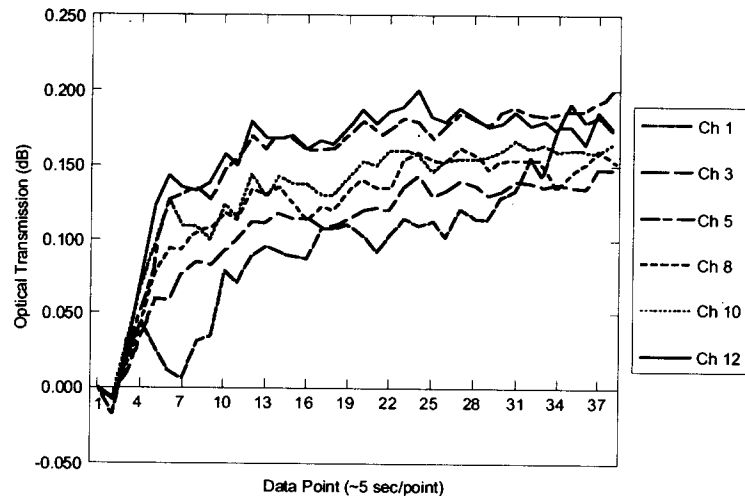


Figure 22. *In situ* optical power transmission during Z-axis vibration of MTP connector assembly.

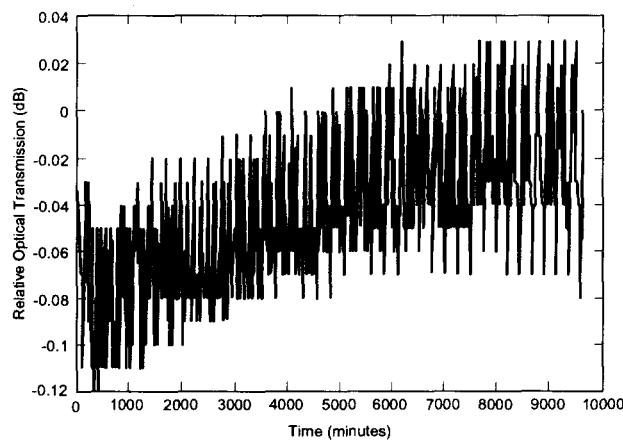


Figure 23. Thermal cycling-induced changes in optical power transmission for MTP connector assembly.

4. CONCLUSIONS

In this paper we have presented a sampling of some of the work on reliability and radiation tolerance of photonics that has taken place recently under the NASA Electronic Parts & Packaging (NEPP) Program. A great deal more work has been conducted within the NEPP Program, both on photonics and in other microelectronics areas, and this work can be accessed on the NEPP Web site at <http://nepp.nasa.gov>. As a conclusion to this brief review, we wish to remark on some common themes emphasized by this work. They are as follows:

1. For both microelectronics and photonics, there is a continuing trend to use more and more COTS components in NASA flight systems. Several factors are responsible for this trend including the simple fact that space qualified and hardened parts are not easily available. In addition, COTS parts often possess greater performance for less cost and quicker delivery. The issue of cost, however, is not always obvious because the added cost of upscreening and radiation testing required to characterize and qualify COTS can result in a greater total cost than that for space level parts. In any case, COTS photonic components will require continuing evaluation before they can be used in NASA systems without jeopardizing mission success.
2. Generally, the radiation issues for photonics that are of most importance for application in the space radiation environment are significantly different from those for Si microelectronics, especially for Si digital microcircuits. For example, with the exception of optical fibers, total ionizing dose (TID) effects are of much less importance for photonics. For III-V-based photonic semiconductor components, displacement damage effects are of greater importance so that the protons in the space environment are a key factor in determining the radiation tolerance for specific mission scenarios. In the case of single event effects (SEE), only the receiver portion of a fiber optic link (FOL) is susceptible, in contrast with Si memory and processor devices.
3. While in some cases it is appropriate to use characterization and qualification methods and techniques employed for Si digital and analog microelectronics as a baseline and "jumping off" point for qualification of photonic components, care must be taken in doing this because the important issues can differ significantly as in the case of radiation effects noted above. Failure mechanisms for photonic components can be quite different from those for Si microelectronics, as can the techniques used to test for and reveal component failure conditions. Thus, care must be taken in not relying too heavily on analogies with the more established qualification techniques used for Si microelectronics.

5. ACKNOWLEDGEMENTS

The authors wish to acknowledge the many contributors to this work and the efforts of the NEPP Program. Many people have contributed to the photonics work under NEPP, and we thank them for their efforts. We also wish to acknowledge the NASA Headquarters Chief Engineer's Office, Code AE, for their support of the NEPP Program.

6. REFERENCES

1. C. Barnes, "The effects of radiation on optoelectronic devices", *SPIE*, **721**, p. 18 (1986).
2. B. Rax, C. Lee, A. Johnston and C. Barnes, "Total dose and proton damage in optocouplers", *IEEE Trans. Nucl. Sci.*, **43**, p. 3167 (1996).
3. R. Reed, P. Marshall, A. Johnston, J. Barth, C. Marshall, K. LaBel, M. D'Ordine, H. Kim and M. Carts, "Emerging optocoupler issues with energetic particle-induced transients and permanent radiation degradation", *IEEE Trans. Nucl. Sci.*, **45**, p. 2833 (1998).
4. A. Johnston and B. Rax, "Proton damage in linear and digital optocouplers", *IEEE Trans. Nucl. Sci.*, **47**, p. 675 (2000).
5. M. O'Bryan, K. LaBel, R. Reed, R. Ladbury, J. Howard Jr., S. Buchner, J. Barth, S. Kniffin, C. Seidleck, C. Marshall, P. Marshall, J. Kim, D. Hawkins, M. Carts, J. Forney, A. Sanders, S. Cox, C. Dunsmore and C. Palor, "Recent radiation damage and single event effect results for candidate spacecraft electronics", *2001 NSREC Workshop Record*, p. 82.
6. T. Miyahira and A. Johnston, "Trends in optocoupler radiation degradation", to be presented at 2002 IEEE NSREC, Phoenix, AZ.
7. A. Johnston and T. Miyahira, "Characterization of proton damage in light emitting diodes", *IEEE Trans. Nucl. Sci.*, **47**, p. 2500 (2000).
8. R. Reed, P. Marshall, C. Marshall, R. Ladbury, H. Kim, L. Nguyen, J. Barth and K. LaBel, "Energy dependence of proton damage in AlGaAs light emitting diodes", *IEEE Trans. Nucl. Sci.*, **47**, p. 2492 (2000).
9. A. Barry, A. Houdayer, P. Hinrichsen, W. Letourneau and J. Vincent, "The energy dependence of lifetime-damage constants in GaAs LEDs for 1 - 500 MeV Protons", *IEEE Trans. Nucl. Sci.*, **42**, p. 2104 (1995).
10. C. Marshall, P. Marshall, M. Carts, R. Reed, S. Baier and K. LaBel, "Characterization of transient error cross sections in high speed commercial fiber optic data links", *2001 IEEE NSREC Workshop Record*, p. 142.
11. C. Marshall, P. Marshall, M. Carts, R. Reed and K. LaBel, "Proton-induced transient effects in a metal-semiconductor-metal (MSM) photodetector for optical-based data transfer", *IEEE Trans. Nucl. Sci.*, **45**, p. 2842 (1998).
12. A. Johnston, T. Miyahira and B. Rax, "Proton damage in advanced laser diodes", *IEEE Trans. Nucl. Sci.*, **48**, p. 1764 (2001).
13. See for example, P. Lyons, L. Looney, H. Henschel, O. Kohn, H. Schmidt, K. Klein, H. Fabian, M. Mills and G. Nelson, "Influence of preform and draw conditions on UV transmission and transient radiation sensitivity on an optical fiber", *SPIE Fiber Optics Reliability: Benign and Adverse Environments III*, **1174**, p. 2 (1989).
14. M. Ott, "Fiber optic cable assemblies for space flight II: thermal and radiation effects", *SPIE Photonics for Space Environments VI*, **3440**, p. 37 (1998).
15. M. Ott and P. Friedberg, "Technology validation of optical fiber cables for space flight environments", *SPIE Optical Devices for Fiber Communications II*, **4216**, p. 206 (2001).
16. M. Ott, "Twelve channel optical fiber connector assembly: from commercial off the shelf to space flight use", available on NEPP Website.
17. M. Bettencourt and M. Ott, "Fiber optic epoxy outgassing study for space flight applications", available on NEPP Website.
18. M. Ott and J. Plante, "Fiber optic cable assemblies for space flight applications: issues and remedies", presented at the 1997 World Aviation Congress and available on the NEPP Web site.
19. J. Plante, M. Ott, J. Shaw and M. Garrison-Darrin, "Draft specification for optical cable, single, multimode fiber, hermetic, loose tube buffer, for space flight", available on the NEPP Web site.
20. J. Plante, "Evaluation report for the Amphenol-Bendix 453 miniature circular connector with Mil-T-29504 optical termini in a vibration environment", available on the NEPP Web site.
21. G. Lutes and M. Tu, "Photonic validation methods handbook", D-18230, available on NEPP Web site.
22. G. Lutes and M. Tu, "Photonic R & QA methods handbook", D-18229, available on NEPP Web site.
23. G. Lutes and M. Tu, "Photonic integration and usage guidelines manual", D-18228, available on NEPP Web site.
24. Q. Kim, C. Wrigley, T. Cunningham and B. Pain, "Space qualification of photonic devices", NEPP Web site.
25. Q. Kim, "Space qualification plan of optoelectronic and photonic devices for optical communication systems", available on NEPP Web site.
26. M. Ott, S. MacMurphy and P. Friedberg, "Characterization of the twelve channel 100/140 micron optical fiber, ribbon cable and MTP array connector assembly for space flight environments", available on NEPP Web site.